Desalination and Water Treatment
www.deswater.com

doi: 10.5004/dwt.2021.26913

220 (2021) 142–151
April

Arsenate removal by chitosan iron oxyhydroxide beads: preparation, characterization, and adsorption studies

J. Ricardo González-Rodríguez[a,*], Oscar Rojas-Carrillo[b], Luis G. Romero-Esquivel[a]

[a]*Environmental Protection Research Center, School of Chemistry, Instituto Tecnológico de Costa Rica, Cartago, Costa Rica, Tel. +50625502791; email: ricardo.gonzalez@tec.ac.cr (J.R. González-Rodríguez), Tel. +50625502568; email: lromero@tec.ac.cr (L.G. Romero-Esquivel)*
[b]*Polymer Research and Technology Laboratory, School of Chemistry, Universidad Nacional, Heredia, Costa Rica, Tel. +5062277-3557; email: oscar.rojas.carrillo@una.ac.cr*

Received 6 August 2020; Accepted 1 December 2020

ABSTRACT

This study compared arsenic removal from drinking water by two different adsorbents: iron-impregnated chitosan beads (Fe-ICB) and iron-doped chitosan beads (Fe-dCB). Scanning electron microscopy, X-ray diffraction (XRD), Fourier transform infrared, and Raman spectroscopy were applied to characterize the materials produced. The As(V) adsorption capacity of both types of materials was evaluated by batch tests, followed by a column test using the most promising material. The XRD and the Raman spectroscopy confirmed the presence of 2-line ferrihydrite in the produced Fe-dCB, and no specific iron oxy-hydroxide was identified in the Fe-ICB. Both types of materials followed either the Langmuir or the Freundlich isotherm adsorption models. The Fe-dCB were more efficient in removing As(V) than the Fe-ICB. The actual maximum capacity of the produced Fe-dCB ranged from 0.27 to 0.61 mg/g under the conditions tested (concentration: 1 mg/L; pH: 7.0; 100 rpm). The Fe-dCB with the better adsorption capacity at low concentrations (<0.1 mg/L) were used in a column test using an As(V) influent concentration of 0.060 mg/L. The Fe-dCB produced close to 91,000 BVs, meeting the standard for drinking water (0.01 mg/L). Therefore, the material exhibits promising adsorbent properties for filtration applications with low arsenic concentrations.

Keywords: Arsenic removal; Chitosan; Iron chitosan beads; Adsorption; Ferrihydrite.

1. Introduction

Groundwater arsenic contamination is a major environmental problem worldwide that affects millions of people and leads to myriad health complications, including several types of cancer as well as neurological and endocrine disorders [1]. Approximately 14 million people in Latin America consume water with arsenic concentrations higher than 10 μg/L, and around 4.5 million people are chronically exposed to concentrations higher than 50 μg/L [2].

Adsorption technology has been widely used to overcome the problem, due to its high removal efficiency, easy operation, and low cost. Numerous adsorbents (e.g., activated alumina, TiO_2, MnO_2, and iron-based adsorbents) have been produced and studied for removing arsenic from drinking water [3]. Iron is the most common metal used in adsorbent production because of its low cost and high arsenic removal capacity [4]. Several iron oxyhydroxides (e.g., goethite, ferrihydrite, and hematite) have received more attention as a result of their high adsorption potentials [5,6]. In addition, according to Thomson et al. [7], adsorption occurs through a bidentate-binuclear bond (Fe–O–As–O–Fe), and the initial interactions are mainly due to electrostatic attraction. However, iron oxyhydroxides

* Corresponding author.

generally need to be granulated for their application in a filtration process, due to their poor mechanical strength and extreme pressure drop.

One simple way to produce an iron-based granulated adsorbent consists of the use of chitosan. This compound is a derivate of chitin, a natural abundant polymer, and has been used as a binding agent or as a base for adsorbent production [8–11]. Chitosan modifications enable the production of crosslinked chitosan, chitosan-coated particles, or chitosan-doped particles. Chitosan-modified adsorbents have been used for the removal of many pollutants, including metal ions, dyes, anions, and phenols [8]. Among these, iron(III)-chitosan beads (Fe-CB) have been developed: specifically, iron(III)-impregnated chitosan beads (Fe-ICB) and iron(III)-doped chitosan beads (Fe-dCB) show promising results for As(III) and As(V) removal in batch systems [11,12].

The Fe-ICB production method consists of gelling the chitosan (dissolving it in a slightly acidic medium, such as acetic acid) and dripping it over NaOH to make the bead shape; the beads are subsequently impregnated by being placed in contact with an iron solution at pH 8 [12]. For Fe-dCB, some studies reported dissolving iron and chitosan in an acid medium and then dropping it over a NaOH solution [11]. However, to date, no study has examined which method is better for arsenic removal. Moreover, knowledge on the effect of loading iron into the chitosan bead surface is limited.

The aim of the current study was to compare two Fe-CB preparation methods in terms of As(V) adsorption capacity using a batch test and to evaluate the behavior of the most promising method at low concentration (0.06 mg/L) using a column test. Furthermore, the chitosan beads were characterized by scanning electron microscopy (SEM), X-ray diffraction (XRD), Fourier transform infrared (FTIR), and Raman spectroscopy to determine the possible iron oxyhydroxides formed during the production procedure.

2. Materials and methods

2.1. Materials

Chitosan was prepared by the Polymer Laboratory (POLIUNA) of Universidad Nacional, Costa Rica, as described below. The sodium hydroxide (Merck, USA), hydrochloric acid (J.T. Baker, 36.5–38%), glacial acetic acid (Merck, USA, 100%), $FeCl_3{\cdot}6H_2O$ (Sigma Aldrich, USA, ≥98%), polyvinyl alcohol (PVA) (Merck, USA, >98%), BES (N,N-Bis(2-hydroxyethyl)-2-aminoethanesulfonic acid (Sigma-Aldrich, USA), and sodium chloride (J.T. Baker) were reagent grade. Arsenate stock solutions were prepared from sodium arsenate $Na_2HAsO_4{\cdot}7H_2O$ (Alfa Aesar, USA, 98%–102%) in ultrapure water and preserved with nitric acid (J.T. Baker, 69%–70%). Atomic absorption spectrometry (AAS) standard solutions were purchased from Sigma-Aldrich (USA).

2.2. Fe-CB synthesis

2.2.1. Chitin and chitosan production

Chitin were extracted following the procedure laid out by Sánchez et al. [13]. Shrimp shell (*Pannaeus vannamei*) was provided by Rainbow Export Processing S.A, Costa Rica. The shells were treated with a 5% sodium hydroxide (NaOH) solution (w/v 1:3) at 298 K for 2 h to remove proteins, lipids, and other organic residues. The deproteinated material was treated with a 5% hydrochloric acid (HCl) solution (w/v 1:2) for 2 h at 298 K to dissolve the inorganic matter. The resulting chitin was then washed and dried.

Chitosan was obtained through chemical deacetylation of the extracted chitin [13]. The material was treated with 50% sodium hydroxide solution (w/v 1:10) for 2 h at 373 K. After the reaction, the produced material was washed with distilled water until near-neutral pH and dried at 333 K in a vacuum oven. The obtained chitosan showed a viscosity-average molecular weight of approximately 137 KDa and a degree of deacetylation (DD) of 75%–80%.

2.2.2. Preparation of the Fe-CB

Fe-CB with varying iron chloride content were prepared using the reagents and concentrations presented in Table 1. The Fe-ICB50 material was prepared using an impregnating method modified from Padilla-Rodríguez et al. [12] with minimal changes in terms of chitosan concentrations (2% w/v vs. 5% w/v in this study) and including the use of PVA. The chitosan was dissolved in an acetic acid solution and then dropped with PVA into the alkaline solution under continuous stirring, in order to form the spherical-shaped beads. The addition of PVA to the alkaline solution induces the formation of well-defined and rounded particles. Thereafter, the chitosan beads were washed with distilled water until they reached neutral pH and were then kept overnight in a 50 mmol/L $FeCl_3$ solution at pH 8 under continuous stirring. The resulting material was washed with deionized water to remove the iron excess and then oven-dried at 45°C for 24 h.

The other materials (Fe-dCB80 to Fe-dCB500) were prepared using a modified doping method from He et al. [11]—varying the $FeCl_3$ molarity from 80 to 500 mmol/L $FeCl_3$, respectively (Table 1); increasing chitosan and acetic acid concentrations from 3% w/v and 1% v/v, respectively, to the concentrations in Table 1; and preparing the gel at environmental temperature instead of at 323 K. The chitosan and $FeCl_3{\cdot}6H_2O$ were dissolved in acetic acid, and the resulting solution was dropped into an alkaline solution under continuous stirring. After 24 h of contact time, all the chitosan beads were rinsed with distilled water until the pH was ~7, and then they were oven-dried at 45°C for 24 h.

2.2.3. Adsorbent characterization

The iron content of the beads was determined by digesting 0.1 g of the material with 20 mL of HNO_3 1+1 at 473 K for 15 min in triplicate. The produced materials were sieved with ASTM standard sieves (N°8 to N°20) to determine the particle size range. The hardness of the samples was tested according to the Mohs scale, using a fingernail and a pocketknife [14]. The surface morphology was observed by means of an SEM—a Hitachi TM-1000 at 1,000x, with 15 kV resolution. The crystalline phase patterns were studied by XRD using a PANalytical (UK) Empyrean device coupled with a PIXcelID detector with CoKα anode

Table 1
Fe-CB synthesis materials and iron contents

Material	Chitosan	Acetic acid	$FeCl_3$ molarity	Alkaline solution	Fe-content
	% w/v	% v/v	mmol/L	% w/v	(mg Fe/g)
Fe-ICB50	5	5	50	2.5% NaOH + 0.5% PVA	2.5[a] ± 0.3[b]
Fe-dCB80	5	5	80	2.5% NaOH	67.2 ± 0.9
Fe-dCB100	4	5	100	2.5% NaOH	92.9 ± 4.1
Fe-dCB150	4	5	150	2.5% NaOH	138.1 ± 2.7
Fe-dCB500	4	5	500	2.5% NaOH	248.7 ± 0.8

[a]Average; [b]standard deviation.

(λ = 1.78901 Å), scanning from 2θ = 5°–80° with a 0.013° step width.

The FTIR spectra of samples were only performed for the Fe-dCB with the highest iron content because the XRD evinces small variations for low iron contents (Fe-ICB50, Fe-dCB80). The spectra were obtained at a resolution of 0.481 cm^{-1} over the range 4,000–400 cm^{-1}, in a Nicolet 380 Thermo Scientific (USA) instrument using an ATR sampling technique. Raman spectra were measured between 200 and 3,500 cm^{-1} using a Thermo Scientific spectrometer (USA), model DXR™, with a laser wavelength of 532.2 nm, with a sampling data space of 0.96 cm^{-1} at 20 times objective. The Raman spectra were carried out only for the Fe-dCB500, due to its high iron content. For SEM images, XRD spectra, and FTIR spectra, a blank consisting of chitosan was also measured in order to contrast the readings.

2.2.4. Isotherm adsorption test

Equilibrium adsorption isotherms were performed by placing different adsorbent doses (between 0.5 and 5 g/L) in contact with 0.2 L of ultrapure water 1 mg/L As(V) solution. The pH was fixed to 7 using 2 mmol/L BES buffer and NaOH or HCl, as recommended by Amy et al. [15]. The test was conducted at 293 K in an orbital shaker, DLab SK-0330-Pro, for 24 h (a suggested equilibration time for Fe-ICB and Fe-dCB) [12,16] and at 100 rpm, which was high enough to ensure well-mixing and avoid vortex formation. The isotherm data were analyzed using the linearized Langmuir and Freundlich adsorption models (Eqs. (1) and (2), respectively):

$$\frac{1}{Q}=\frac{1}{Q_m}+\frac{1}{Q_m b}\left(\frac{1}{C}\right) \tag{1}$$

where Q is the equilibrium adsorption capacity (mg/g), Q_m is the Langmuir maximum adsorption capacity (mg/g), b is the Langmuir constant (L/mg), and C is the equilibrium concentration (mg/L).

$$\log Q=\log K_F+n\log C \tag{2}$$

where Q is the equilibrium adsorption capacity (mg/g), K_F is the Freundlich adsorption capacity parameter (mg/g) $(L/mg)^n$, C is the equilibrium concentration (mg/L), and n is the Freundlich adsorption intensity parameter (arbitrary units).

2.2.5. Breakthrough curve column test

The breakthrough curve (BTC) test was conducted using a plastic column (28.5 mm × 200 mm, W × L) at room temperature. Ultrapure water was spiked with an initial As(V) concentration of ~0.06 mg/L, the ionic strength was controlled with 15 mmol/L NaCl, and the influent pH was 5.6 since no buffer was added. The solution was pumped upflow through the system at 1.0 m/h using a dosing pump (Hannah Instruments, USA, model BL 10) to maintain an empty bed contact time (EBCT) of 5 min, as suggested by Rubel [18]. Prior to use, the material was kept in distilled water for 24 h to swell the particles. Then, the column was packed carefully using the wet method in order to avoid the introduction of air bubbles [19]. Glass beads were placed above and below the material to disperse the flow, as recommended by Hristovski et al. [20]. 20 mL effluent samples were taken at different time intervals for arsenic analysis. The experiment lasted approximately 15 months, until the effluent arsenic concentration was above the maximum contaminant level (MCL) of 0.01 mg/L.

2.3. Analytical methods

The iron and arsenic determinations were performed using an atomic absorption spectrometer (Perkin Elmer, model Analyst 800) according to the Standard Methods for the Examination of Water and Wastewater method 3111B (direct air–acetylene flame method) and method 3114B (hydride generation method), respectively [21]. The instrument measurement of each sample was performed in duplicate. The detection limits were 0.2 mg/L and 1 μg/L for iron and arsenic, respectively. Samples were preserved at pH < 2 using HNO_3 and stored at 277 K until they were analyzed. To avoid contamination, all bottles, glassware, and columns were rinsed with HNO_3 1+1 and then with ultrapure water.

3. Results and discussion

3.1. Characterization of the Fe-CB

The resulting materials were insoluble in water and showed high hardness (2.5–5, Mohs scale) and a uniform rounded shape, with a grain size of 0.85–1.7 mm. The

impregnated beads, called Fe-ICB50, had a light orange surface color; the iron(III)-doped chitosan beads (Fe-dCB80 to Fe-dCB500) had the appearance of brownish granules. Both colors are evidence of the presence of iron.

Table 1 shows the amount of iron(III) loaded into the beads. Fe-ICB50 presented a low iron content (2.5 mg/g), showing that the impregnated method is less efficient. Fe-dCB80 to Fe-dCB500 presented a greater iron content—from 67.2 to 248.7 mg/g—showing that the iron uptake is improved with this technique and that it is a function of the iron chloride molarity used (Table 1). For comparison, the Fe-ICB50 iron content in this study is slightly lower than that produced by Padilla-Rodríguez et al. [12], at 6.3 mg/g. This suggests that the iron loading into the bead is not dependent on the chitosan ratio, but rather seems to be surface dependent. In terms of Fe-dCB, the Fe-dCB150, and Fe-dCB500 showed higher iron contents (138.1 and 248.1 mg/g, respectively) than that reported by He et al. [11], at 127.78 mg/g.

Fig. 1 shows the SEM images at 1,200x of the raw chitosan and at 1,000x of the Fe-CB produced. As can be seen, the chitosan (Fig. 1a) has a slightly rough surface, which was seen in each of the beads produced, primarily at higher iron contents. The Fe-ICB50 and Fe-dCB80 (Figs. 1b and c) showed small surface changes compared to the pure chitosan, and the Fe-dCB100 and Fe-dCB150 showed a rougher and irregular surface. With regard to Fe-dCB500, a different pattern can be observed compared to the others: some particles can be seen attached to the surface. This suggests that the iron chloride concentration (500 mmol/L) used in the synthesis was excessive, and iron oxyhydroxide probably precipitated on the surface.

Fig. 2 shows the chitosan and Fe-CB FTIR spectra. Characteristic chitosan bands are identified as the N–H stretching at 3,360 cm^{-1}, the C–H stretching at 2,875 cm^{-1}, the amide group at 1,650 cm^{-1}, the amino group at 1,577 cm^{-1} (absent in chitin), the amide methyl group at 1,379 cm^{-1}, the C–O–C stretching at 1,152 cm^{-1}, and the C–O stretching at 1,020 cm^{-1} [22,23]. These bands are also exhibited in the iron composite beads. However, with Fe-CB500, a decrease in the intensity of the chitosan characteristic bands is noted, suggesting a metal-polymer complexation. Interestingly, the transmittance of the N–H band at 3,360 cm^{-1} of the C-2-amino is substantially reduced in Fe-CB500, which has higher iron loading (Table 1), showing an interaction between the metal and the amino group and a possible complexion taking place into the hydrophilic pocket of the polymer. Nevertheless, the characterization of the iron oxyhydroxide by this technique was impossible, since the bands of the Fe–O bonds between 600 and 1,000 cm^{-1} were unclear as a result of chitosan interference (Fig. 2).

XRD analysis was performed to compare the produced Fe-CB with the chitosan raw material (Fig. 3a). The raw chitosan showed two broad peaks, at 2θ = 9°–13° and at 20°–28°. The peak at 9°–13° is related to the amorphous portion of the chitosan structure, due to the presence of amino groups at C-2-amino; the peak at 20°–28° is related

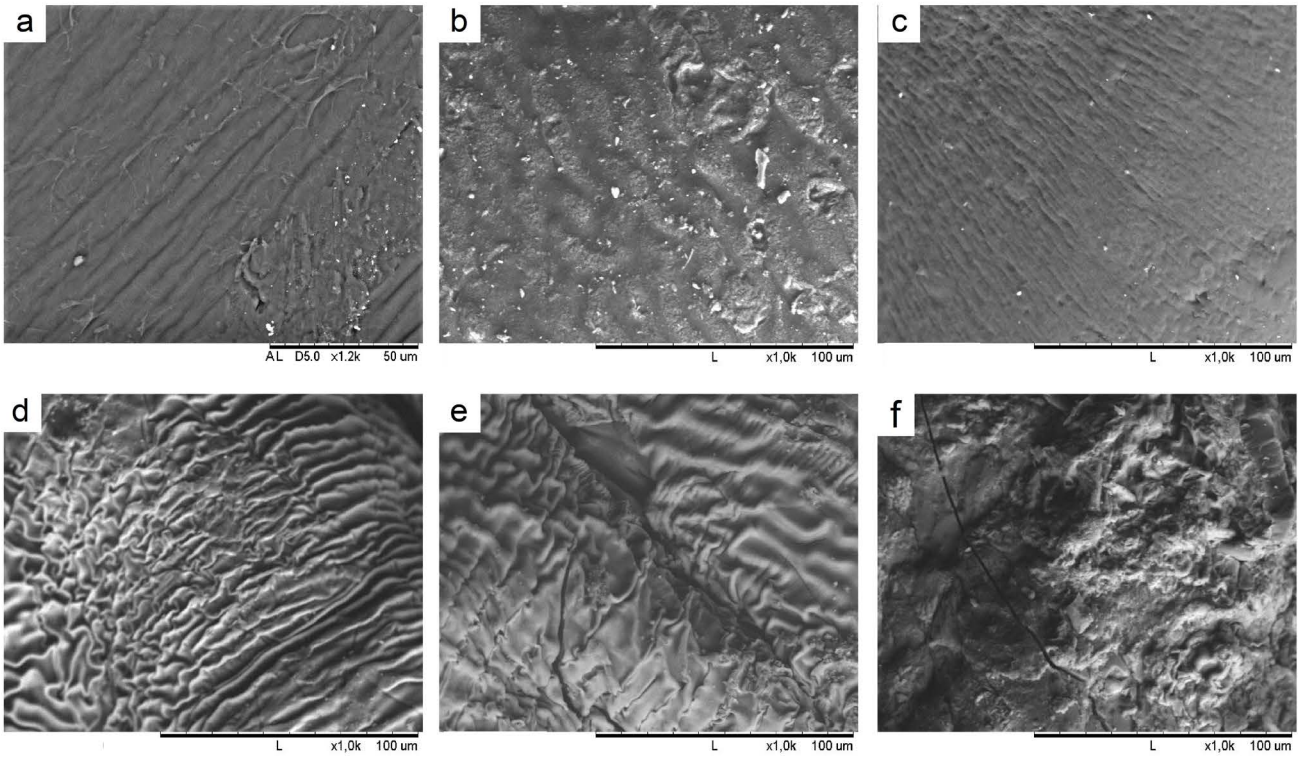

Fig. 1. SEM micrographs from chitosan and different Fe-CB: (a) chitosan, (b) Fe-ICB50, (c) Fe-dCB80, (d) Fe-dCB100, (e) Fe-dCB150, and (f) Fe-dCB500.

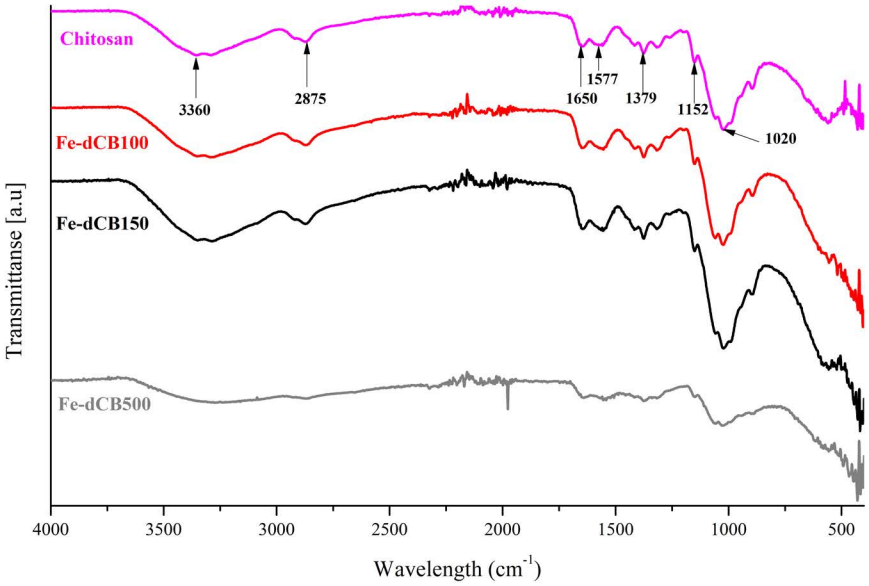

Fig. 2. FTIR spectra of the Fe-dCB100, Fe-dCB150, and Fe-dCB500.

to the crystalline portion of the biopolymer structure, resulting from packing of the polymer chain and interchain interactions [24]. The Fe-ICB50 diffractogram is very similar to the raw chitosan, indicating an unnoticeable change in the structure by the iron(III) impregnation. In contrast, the XRD pattern of the iron(III)-doped materials (Fe-dCB80 to Fe-dCB500) showed attenuation in the chitosan peaks at 9°–13° and at 20°–28°. This indicates that the structure of the chitosan was transformed into a more amorphous structure when it was doped with iron(III). When the chitosan is loaded with iron, the hydrogen bonds between the C-2-amino and hydroxyl bounds can be disrupted, and thus the polymer chains become disordered and more amorphous [10,24]. This finding supports the results found in the FTIR spectra, where the transmittance of the N–H band at 3,360 cm^{-1} of the C-2-amino decreased as the iron content increased.

In addition, the Fe-CB materials from Fe-dCB100 on showed a new poor amorphous phase, with two broad peaks at 41° and 74° (Fig. 3a). The trend in the intensity of these peaks correlates to the iron loading in the beads (i.e., the intensity increases as the iron loading increases). According to Cornell and Schwertmann [25], such peaks are related to 2-line ferrihydrite. Fig. 3b shows the diffractogram of the Fe-dCB500 and of a synthetic ferrihydrite produced by Gimsing and Borggaard [26]. As can be seen, the patterns are similar despite interference from chitosan. This finding is further supported by Raman spectroscopy.

The Raman spectra of the produced materials were conducted to confirm the presence of the 2-line ferrihydrite in the Fe-dCB evidenced in the XRD. The use of Raman spectroscopy is appropriate for minerals that display poorly-defined XRD patterns, like ferrihydrite [27]. Fig. 4a shows the Fe-dCB500 and the chitosan (70% DD) spectra reported

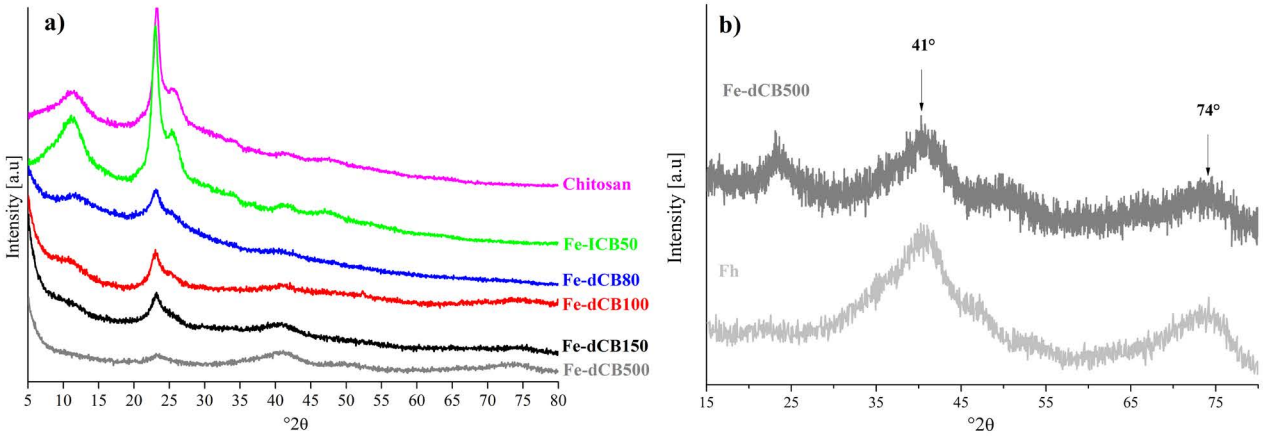

Fig. 3. XRD of (a) the Fe-CB produced in this study and (b) Fe-dCB500, with the synthetic ferrihydrite of Gimsing and Borggaard [26].

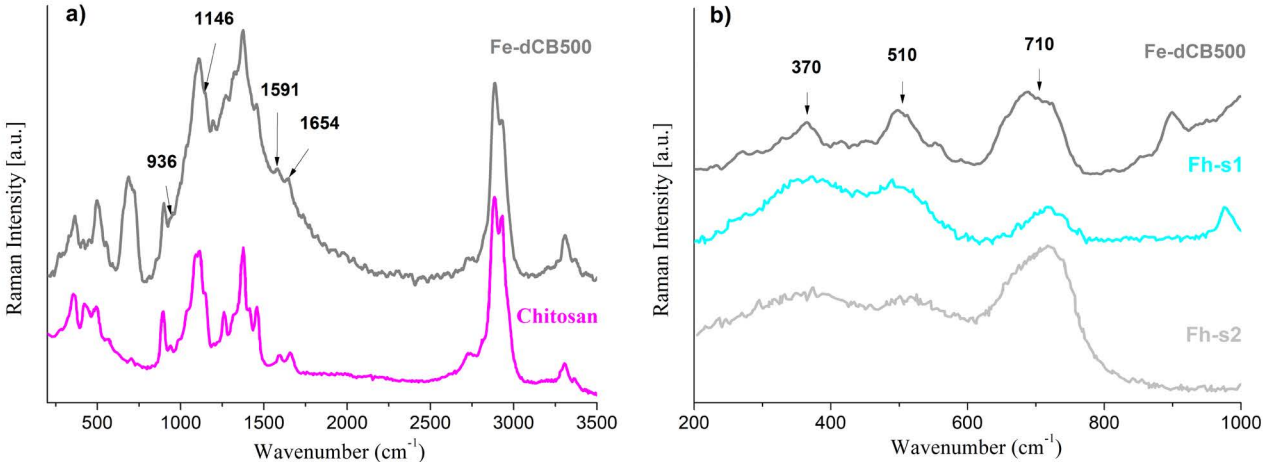

Fig. 4. Raman spectroscopy of Fe-dCB500 compared to: (a) chitosan from Zajaç et al. [28] and two synthetic ferrihydrite and (b) Fh-s1 from Zhang et al. [30] and Fh-s2 from Mazzetti and Thistlethwaite [31].

by Zajaç et al. [28]. The characteristic Raman bands of chitosan found in Fe-dCB500 are the stretching vibrations at 936 cm^{-1} (C=O), at 1,146 cm^{-1} (C–O–C), and at 1,654 cm^{-1} (CN), as well as the bending vibrations at 1,591 cm^{-1} (NH_2) [28,29]. Furthermore, the spectra of the Fe-dCB500 exhibits three bands related to the iron oxyhydroxy phase below 1,000 cm^{-1} (Fig. 4b). It shows two broad and weak bands at 370 and 510 cm^{-1} and a stronger one at 710 cm^{-1}, which is consistent with the findings of synthetic 2-line ferrihydrite (Fh-s1 and Fh-s2) produced by Zhang et al. [30] and by Mazzetti and Thistlethwaite [31], respectively.

Using a similar bead production methodology, He et al. [11] found that ferrihydrite and goethite were both presents in the beads. It is important to note that the characterization methods used in this study (XDR, FTIR, and Raman spectroscopy) were not used by them, which could provide a valuable comparison opportunity. They detected a mixture of nano-ferrihydrite and nano-goethite using zero-field ^{57}Fe Mossbauer spectroscopy, but the proportion of each compound was unknown. In contrast, in the present study, the XRD and Raman only suggest the presence of 2-line ferrihydrite.

3.2. Isotherm adsorption test

Adsorption isotherm tests were performed in order to study the adsorption to the produced Fe-CB. Fig. 5 shows the isotherm data and the best fit model (Langmuir or Freundlich) according to the R^2 in Table 2. Closer examination of Fig. 5 reveals that the As(V) adsorption of the Fe-ICB50 material was significantly lower than the Fe-dCB materials, indicating that the Fe-dCB production procedure leads to more efficient material. Among those materials, several differences in the As(V) adsorption curves suggest that iron uptake plays a role in the adsorption process.

As can be seen in the Fig. 5 inset, the adsorption is relatively similar for all Fe-dCB below 0.1 mg/L of As(V) equilibrium concentration; only Fe-dCB150 presented slightly higher adsorption. Interestingly, at equilibrium concentrations higher than 0.1 mg/L of As(V), Fe-dCB500—the material with the highest iron content (248.7 mg/g, Table 1)—presented a plateau, as well as the lowest adsorption capacity among the Fe-dCBs at all equilibrium concentrations above 0.1 mg/L. In contrast, Fe-dCB80, Fe-dCB100, and Fe-dCB150 presented similar capacities between As(V) equilibrium concentrations of 0.10–0.25 mg/L; above that range, Fe-dCB100 performed slightly better. Therefore, among those materials, a trend between the iron loading and the adsorption capacity was undetected. For Fe-dCB500, the decrease in the adsorption capacity compared to the other Fe-dCBs may have occurred due to a blockage in the pathways to adsorption sites caused by the precipitates observed in Fig. 1f. The use of Fe-dCB150 and Fe-dCB100 could be recommended for concentrations lower and higher than 0.1 mg/L of As(V), respectively.

The adsorption isotherm parameters are shown in Table 2. The Fe-ICB50 fits better to the Langmuir model, consistent with Padilla-Rodríguez et al.'s [12] findings for a similar material, indicating a mono-layer coverage of the As(V) on the Fe-ICB [18]. The Fe-ICB50 in this study showed lower Q_m (1.75 mg/g) than the finding of Padilla-Rodríguez et al. [12] (at 2.72 mg/g). The better performance of their study could be due to a higher iron content of the beads (6.3 vs. 2.5 mg/g), a lower equilibrium pH (6.0 vs. 7.0) that favors arsenic adsorption, and probably the present study's higher initial arsenic concentration range (up to 5 vs. 1 mg/L).

Regarding the Fe-dCB (Fig. 5), the Fe-dCB500 presented a maximum capacity plateau or L-shape and thus fits better to the Langmuir model (see R^2 in Table 2). In contrast, the other Fe-dCBs better follow the Freundlich model, showing high affinity ($n < 1$) or favorable adsorption at lower equilibrium concentrations [17]. The n value range is 0.69–0.89 (Fe-dCB150 < Fe-dCB80 < Fe-dCB100), indicating that the latter performed better at higher arsenic equilibrium concentrations, as shown in Fig. 5.

The experimental or actual maximum capacity, Q_{max}, of the Fe-dCBs (Fig. 5) ranged between 0.27 and 0.61 mg/g

Table 2
Isotherm parameters for As(V) uptake on the different chitosan beads produced

Material	Langmuir			Freundlich		
	Q_m (mg/g)	b (L/mg)	R^2	K_F (mg/g)(L/mg)^n	n	R^2
Fe-ICB50	1.75	0.1	0.643	0.17	0.84	0.574
Fe-dCB80	1.31	0.9	0.981	0.76	0.84	0.992
Fe-dCB100	3.66	0.3	0.932	0.94	0.89	0.936
Fe-dCB150	0.76	2.2	0.961	0.67	0.69	0.988
Fe-dCB500	0.35	3.7	0.930	0.31	0.46	0.914

Q_m: maximum adsorbent capacity; b: Langmuir adsorption coefficient; K_F: Freundlich adsorption intensity coefficient; n: Freundlich affinity exponent.

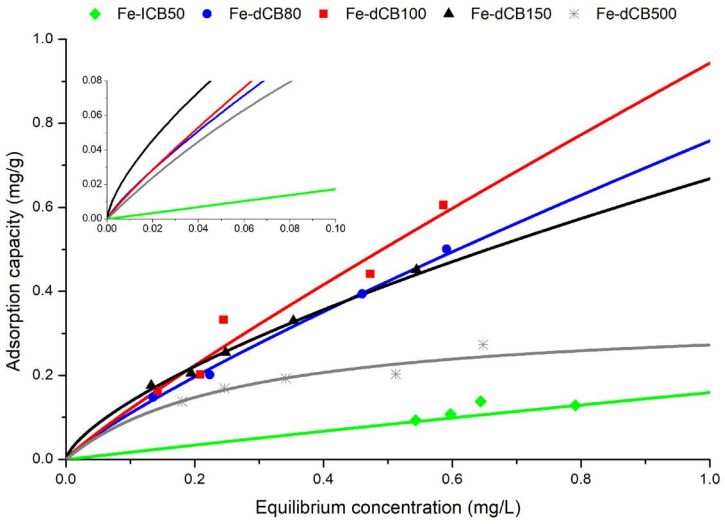

Fig. 5. Best fit isotherms of Fe-ICB50, Fe-dCB80, Fe-dCB100, Fe-dCB150, and Fe-dCB500. Inset: isotherms' behavior at low range concentrations.

(Fe-dCB500 < Fe-dCB150 < Fe-dCB80 < Fe-dCB100). As shown in Table 3, Fe-dCB100 presented a higher capacity than the low-cost material rice husk biochar and a similar capacity to chitosan red scoria blend and laterite soil. Compared with other similar Fe-dCBs, Fe-dCB100 showed a slightly lower adsorption capacity than iron-doped chitosan granules, and one order of magnitude lower than goethite chitosan beads and chitosan-iron oxyhydroxide beads. The higher capacities reported by He et al. [11] and Hasan et al. [16] when using those materials can be related to their higher equilibrium concentrations of 5–63 mg/L and 1–50 mg/L of As(V), respectively, used in the batch experiments. Additionally, Hasan et al. [16] and He et al. [11] used lower pH values (6.5 and 5.0, respectively), which is a condition that favors the adsorption capacity for iron oxyhydroxides [32]. In summary, the batch test results suggest good adsorption performance with a more realistic arsenic concentration than those evaluated in previous studies for Fe-dCBs.

3.3. Column filtration test

Given that Fe-dCB150 presented a relatively better potential at low concentrations (Fig. 5, inset), and given its higher Freundlich affinity to As(V) (between the best-fit materials to Freundlich model) (Table 2), it was chosen for the evaluation of the removal capacity in the column filtration mode.

Fig. 6 shows the As(V) BTC of the Fe-dCB150 material for 0.06 mg/L As(V) influent concentration. At the beginning of the BTC (<20,000 BV), an atypical effluent arsenic plume was detected close to the MCL. That effect is related to a reduction in the adsorption capacity of the material, probably due to some alkali residuals that remained after the bead washing and that increase the water pH and therefore decrease the adsorption capacity [37]. This indicates that for future application and scale-up, the beads require an efficient washing step in the production phase and/or extensive monitoring at effluent. Above 20,000 BV, the arsenic stabilized to zero, and then the curve started to show the characteristic *S*-shape of a BTC. The breakthrough at the MCL (BV_{10}) was around 91,000 BVs.

Few studies have reported Fe-dCB column studies. Hasan et al. [16] reported a column test for Fe-dCB using an inlet ultrapure water solution of 10 mg/L of total arsenic (5 mg/L As(V) + 5 mg/L As(III)) and could treat 50 BVs for As(V) at BV_{10}. Gupta et al. [36], using glutaraldehyde crosslinked

Table 3
Comparison of the adsorption of As(V) by Fe-dCB and other low-cost adsorbents

Material	C_0 (mg/L)	pH	Q_{max} (mg/g)	Reference
Rice husk biochar	0.09–0.85	6.7	0.014	[33]
Chitosan red scoria blend	0.1–10	7	0.62	[34]
Laterite soil	0.1–25	7	0.63	[35]
Iron-doped chitosan granules	1–10	7	0.84	[36]
Goethite chitosan beads	5–63	5	8.50	[11]
Chitosan-iron oxyhydroxide beads	1–50	6.5	4.95	[16]
Fe-dCB100	1	7	0.61	This study

C_0: Initial concentration; Q_{max}: actual maximum capacity reported.

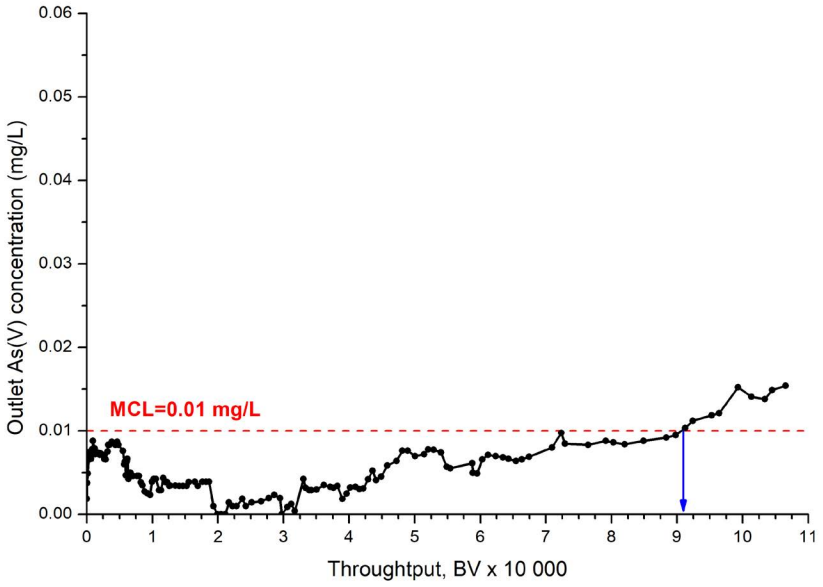

Fig. 6. Breakthrough curve of Fe-dCB150.

Fe-dCB, reported a BV_{10} of 112 BVs for groundwater, with an initial concentration of 0.5 mg/L. The Fe-dCB150 in the current study showed a larger amount of BV_{10} (91,000 BVs) than both studies. Despite the differences in As concentrations, water type, and pH (7.0 vs. 5.6 in this study), the Fe-dCB150 performed much better than the other studies.

Given these column results, it is interesting to compare the Fe-dCB150 performance with commercial iron-based adsorbents. Zeng et al. [38] used a synthetic ferrihydrite (Enviroscrub Technologies Corporation, USA) and reported a BV_{10} of 32,400 BVs, with an influent concentration of 0.1 mg/L at pH 7.5 with ultrapure water. Barlokova et al. [39] reported 28,600 BVs for As(V) at BV_{10} in a column study for Bayoxide® E33 (90.1% α-FeOOH) using tap water spiked with an inlet concentration of 0.05 mg/L at neutral pH. The ferrihydrite and the E33 had almost 2.8 and 3.2 times lower BV_{10} than Fe-dCB150, respectively. Although the experimental conditions (e.g., pH and water type) are quite different, with a similar arsenic influent concentration the Fe-dCB150 clearly presents a similar or higher adsorption capacity to those commercial products.

4. Conclusion

Effective arsenic removal using Fe-CB materials has been reported in the literature with two different production methods, leading to Fe-dCB and Fe-ICB. The aim of the present study was to demonstrate under identical evaluation conditions which produced material performs better. The results demonstrated that Fe-dCB is more efficient for arsenic removal than Fe-ICB. Moreover, in Fe-dCBs, the interaction of the iron oxyhydroxides formed with the chitosan matrix was supported by XRD and FTIR measurements. Furthermore, XRD and Raman tests confirmed the presence of 2-line ferrihydrite in the Fe-dCB chitosan beads.

In addition, batch adsorption studies indicated that arsenic adsorption better followed the Freundlich model and that the capacity of the Fe-dCBs is relatively similar among the materials, with iron uptakes between 67 and 138 mg/g. However, when the iron content was close to 250 mg Fe/g (Fe-dCB150), the adsorption presented a maximum limited adsorption capacity and followed the Langmuir model, showing that high iron uptakes might limit the arsenic access to the adsorption sites, probably due to iron precipitates.

The column test showed that the Fe-dCB150 presented a superior performance to the BV_{10} than similar Fe-CB results previously reported. The number of BVs treated by Fe-dCB150 is even higher than commercial adsorbents in the tested conditions. Therefore, results suggest that the iron composite chitosan beads produced are promising for upscaled production.

Acknowledgments

This research was funded by the Research and Extension Council of ITCR, project no. 1460–044.

Symbols

Q — Equilibrium adsorption capacity
Q_m — Langmuir maximum adsorption capacity
Q_{max} — Actual maximum capacity reported
b — Langmuir adsorption intensity parameter
C — Equilibrium concentration
K_F — Freundlich adsorption capacity parameter
n — Freundlich adsorption intensity parameter

References

[1] P. Pal, M. Sen, A. Manna, J. Pal, P. Pal, S. Roy, P. Roy, Contamination of groundwater by arsenic: a review of occurrence, causes, impacts, remedies and membrane-based purification, J. Integr. Environ. Sci., 6 (2009) 295–316.
[2] R. Kumar, M. Patel, P. Singh, J. Bundschuh, C.U. Pittman, L. Trakal, D. Mohan, Emerging technologies for arsenic removal from drinking water in rural and peri-urban areas: methods, experience from, and options for Latin America, Sci. Total Environ., 694 (2019) 1–26, doi: 10.1016/j.scitotenv.2019.07.233.
[3] D. Mohan, C.U. Pittman, Arsenic removal from water/wastewater using adsorbents - a critical review, J. Hazard. Mater., 142 (2007) 1–53.
[4] M.E. Sigrist, H.R. Beldomenico, E.E. Tarifa, C.L. Pieck, C.R. Vera, Modelling diffusion and adsorption of As species in Fe/GAC adsorbent beds, 86 (2011) 1256–1264.
[5] Y. Mamindy-Pajany, C. Hurel, N. Marmier, M. Roméo, Arsenic adsorption onto hematite and goethite, C.R. Chim., 12 (2009) 876–881.
[6] F. Li, D. Geng, Q. Cao, Adsorption of As(V) on aluminum-, iron-, and manganese-(oxyhydr)oxides: equilibrium and kinetics, Desal. Water Treat., 56 (2015) 1829–1838.
[7] B. Thomson, A. Aragon, J. Anderson, J. Chwirka, P. Brady, Rapid Small Scale Column Testing for Evaluating Arsenic Adsorbents, Water Research Foundation, 2005.
[8] A. Bhatnagar, M. Sillanpää, Applications of chitin- and chitosan-derivatives for the detoxification of water and wastewater - a short review, Adv. Colloid Interface Sci., 152 (2009) 26–38.
[9] S. Shahraki, H.S. Delarami, F. Khosravi, Synthesis and characterization of an adsorptive Schiff base-chitosan nanocomposite for removal of Pb(II) ion from aqueous media, Int. J. Biol. Macromol., 139 (2019) 577–586.
[10] M. Vakili, S. Deng, D. Liu, T. Li, G. Yu, Preparation of aminated cross-linked chitosan beads for efficient adsorption of hexavalent chromium, Int. J. Biol. Macromol., 139 (2019) 352–360.
[11] J. He, F. Bardelli, A. Gehin, E. Silvester, L. Charlet, Novel chitosan goethite bionanocomposite beads for arsenic remediation, Water Res., 101 (2016) 1–9.
[12] A. Padilla-Rodríguez, O. Perales-Pérez, F.R. Román-Velázquez, Removal of As(III) and As(V) oxyanions from aqueous solutions by using chitosan beads with immobilized Iron(III), Int. J. Hazard. Mater., 2 (2014) 7–17.
[13] A. Sánchez, M. Sibaja, J. Vega-Baudrit, S. Madrigal, Síntesis y caracterización de hidrogeles de quitosano obtenidos a partir del camáron langostino (*Pleuroncodes planipes*) con potenciales aplicaciones biomédicas, Rev. Iberoam. Polímeros, 8 (2007) 241–267.
[14] K.J. Anderson, Hardness testing, Mater. Res. Soc. Bull., 19 (1994) 76–77.
[15] G. Amy, H.C. Chen, A. Drizo, U. von Gunten, P. Brandhuber, R. Hund, Z. Chowdhury, S. Kommineni, S. Shahnawaz, M. Jekel, K. Banerjee, Adsorbent Treatment Technologies for Arsenic Removal, American Water Works Association, Denver, 2005.
[16] S. Hasan, A. Ghosh, K. Race, R. Schreiber, M. Prelas, Dispersion of FeOOH on chitosan matrix for simultaneous removal of As(III) and As(V) from drinking water, Sep. Sci. Technol., 49 (2014) 2863–2877.
[17] E. Worch, Adsorption Technology in Water Treatment: Fundamentals, Processes, and Modeling, Walter de Gruyter, Dresden, 2012.
[18] F. Rubel, Design Manual: Removal of Arsenic from Drinking Water by Adsorptive Media, Ohio, 2003.
[19] T. Kawakita, J. Fujiki, K. Tsubomatsu, E. Furuya, A simple determination method of adsorption kinetics from a liquid phase fixed-bed breakthrough curve, Chem. Eng. Technol., 36 (2013) 259–267.
[20] K.D. Hristovski, P.K. Westerhoff, J.C. Crittenden, L.W. Olson, Arsenate removal by nanostructured ZrO_2 spheres, Environ. Sci. Technol., 42 (2008) 3786–3790.
[21] APHA, AWWA, WEF, Standard Methods for Examination of Water and Wastewater, American Public Health Association, Washington, DC, 2005.
[22] K. Yao, J. Li, F. Yao, Y. Yin, Chitosan-Based Hydrogels: Functions and Applications, CRC Press, New York, NY, 2012.
[23] I.K.D. Dimzon, T.P. Knepper, Degree of deacetylation of chitosan by infrared spectroscopy and partial least squares, Int. J. Biol. Macromol., 72 (2015) 939–945.
[24] A. Webster, M.D. Halling, D.M. Grant, Metal complexation of chitosan and its glutaraldehyde cross-linked derivative, Carbohydr. Res., 342 (2007) 1189–1201.
[25] R.M. Cornell, U. Schwertmann, The Iron Oxides Structure, Properties, Reaction, Ocurrences and Uses, Wiley-VCH GmbH and Co., KGaA, Weinheim, 2003.
[26] A.L. Gimsing, O.K. Borggaard, Phosphate and glyphosate adsorption by hematite and ferrihydrite and comparison with other variable-charge minerals, Clays Clay Miner., 55 (2007) 108–114.
[27] M. Hanesch, Raman spectroscopy of iron oxides and (oxy) hydroxides at low laser power and possible applications in environmental magnetic studies, Geophys. J. Int., 177 (2009) 941–948.
[28] A. Zajaç, J. Hanuza, M. Wandas, L. Dymińska, Determination of N-acetylation degree in chitosan using Raman spectroscopy, Spectrochim. Acta, Part A, 134 (2015) 114–120.
[29] X.D. Ren, Q.S. Liu, H. Feng, X.Y. Yin, The characterization of chitosan nanoparticles by raman spectroscopy, Appl. Mech. Mater., 665 (2014) 367–370.
[30] D. Zhang, S. Wang, Y. Wang, M.A. Gomez, Y. Duan, Y. Jia, The transformation of two-line ferrihydrite into crystalline products: effect of pH and media (sulfate versus nitrate), ACS Earth Space Chem., 2 (2018) 577–587.
[31] L. Mazzetti, P.J. Thistlethwaite, Raman spectra and thermal transformations of ferrihydrite and schwertmannite, J. Raman Spectrosc., 33 (2002) 104–111.
[32] A. Jain, R.H. Loeppert, Effect of competing anions on the adsorption of arsenate and arsenite by ferrihydrite, J. Environ. Qual., 29 (2000) 1422–1430.
[33] E. Agrafioti, D. Kalderis, E. Diamadopoulos, Arsenic and chromium removal from water using biochars derived from rice husk, organic solid wastes and sewage sludge, J. Environ. Manage., 133 (2014) 309–314.
[34] T.G. Asere, S. Mincke, J. De Clercq, K. Verbeken, D.A. Tessema, F. Fufa, C.V. Stevens, G. Du Laing, Removal of arsenic(V) from aqueous solutions using chitosan–red scoria and chitosan–pumice blends, Int. J. Environ. Res. Public Health, 14 (2017) 1–19.

[35] T.H. Nguyen, H.N. Tran, H.A. Vu, M.V. Trinh, T.V. Nguyen, P. Loganathan, S. Vigneswaran, T.M. Nguyen, V.T. Trinh, D.L. Vu, T.H.H. Nguyen, Laterite as a low-cost adsorbent in a sustainable decentralized filtration system to remove arsenic from groundwater in Vietnam, Sci. Total Environ., 699 (2020) 1–11, doi: 10.1016/j.scitotenv.2019.134267.
[36] A. Gupta, V.S. Chauhan, N. Sankararamakrishnan, Preparation and evaluation of iron-chitosan Composites for removal of As(III) and As(V) from arsenic contaminated real life groundwater, Water Res., 43 (2009) 3862–3870.
[37] Z. Yin, J. Lützenkirchen, N. Finck, N. Celaries, K. Dardenne, H.C.B. Hansen, Adsorption of arsenic(V) onto single sheet iron oxide: X-ray absorption fine structure and surface complexation, J. Colloid Interface Sci., 554 (2019) 433–443.
[38] H. Zeng, M. Arashiro, D.E. Giammar, Effects of water chemistry and flow rate on arsenate removal by adsorption to an iron oxide-based sorbent, Water Res., 42 (2008) 4629–4636.
[39] D. Barlokova, J. Ilavsky, M. Marton, M. Kunstek, Removal of heavy metals in drinking water by iron-based sorption materials, IOP Conf. Ser.: Earth Environ. Sci., 362 (2019) 1–12, doi: 10.1088/1755-1315/362/1/012109.